

Peaks of sound velocity in two color dense QCD: quark saturation effects and semishort range correlations

Toru Kojo^{1,*} and Daiki Suenaga^{2,†}

¹*Key Laboratory of Quark and Lepton Physics (MOE) and Institute of Particle Physics,
Central China Normal University, Wuhan 430079, China*

²*Research Center for Nuclear Physics, Osaka University, Ibaraki, 567-0048, Japan*
(Dated: March 29, 2022)

We discuss stiffening of dense matter in two color QCD (QC₂D) where hadrons are mesons and diquark baryons. We study two models which describe a transition of matter from the Bose-Einstein-Condensation regime at low density to the Bardeen-Cooper-Schrieffer regime at high density. The first model is based on coherent states of diquarks, and the second is the Nambu-Jona-Lasinio model with diquark pairing terms. We particularly focus on how quark states are occupied as baryon density increases. We find that, due to the occupied quark levels, the ideal gas picture of diquarks breaks down at density significantly less than the density where baryon cores overlap. The saturation of quark states at low momenta stiffens equations of state. We also study the effects of interactions which depend on the quark occupation probability. We argue that equations of state become very stiff when the bulk part of the quark Fermi sea has the effective repulsion but the Fermi surface enjoys the attractive correlations. This disparity for different momentum domains is possible due to the strong channel dependence in gluon exchanges with momentum transfer of 0.2 – 1 GeV. These concepts can be transferred from QC₂D to QCD in any numbers of colors.

I. INTRODUCTION

The quantum chromodynamics (QCD) with two colors $N_c = 2$ (QC₂D) has been a useful laboratory to test theoretical conceptions in dense matter [1–19]. In this theory, hadrons are mesons and diquark baryons. At low baryon density, the dilute matter is dominated by diquark baryons, and it continuously transforms into a matter dominated by quarks. In the literatures, this continuous transformation is often referred as the crossover from Bose-Einstein-Condensation (BEC) phase to Bardeen-Cooper-Schrieffer (BCS) phase [20? ?]. For even flavors, the path-integral of QC₂D has the positive measure so that the lattice Monte Carlo simulations are doable [21–40]. In this paper, we use QC₂D in two flavors ($N_f = 2$) to discuss some concepts which have been proposed for QCD to account for the neutron star (NS) phenomenology.

The quark-hadron continuity realized in QC₂D can give important clues to understand recent findings in NS observations [41–52]. Recent analyses of NSs, with similar radii ($\simeq 12.4$ km) for 2.1 and 1.4 solar mass NSs [50–52], imply that strong first order phase transitions are disfavored for a density between nuclear saturation density n_0 (~ 0.16 fm⁻³) and the core baryon density realized in two-solar mass NSs, $n_B = 4 - 7n_0$. For this reason the quark-hadron continuity (modulo weak first order transitions) can be a useful baseline to describe the QCD equation of state (EoS) [53], and it is important to

understand how such a continuous transition proceeds microscopically.

In QCD, early constructions on NS EoS with the continuity scenario were largely based on phenomenological interpolations between hadronic and quark EoS [54–66]. They found several qualitative trends, such as a peak in the sound velocity, relatively large strangeness fraction at $n_B \simeq 5n_0$, and the importance of semi-short range correlations. While these trends in QCD remain conjectures, in QC₂D one can directly test these concepts on the lattice. In this paper we use QC₂D to discuss how stiffening of matter takes place in the quark-hadron continuity.

Rapid stiffening of dense matter was discussed by McLerran and Reddy in a quarkyonic matter model [67]. Quarkyonic matter is basically a quark matter, but with baryons near the quark Fermi surface [68–78]. In the presence of the quark Fermi sea, the quark Pauli blocking effects force baryons to take large momenta, $P_B \sim N_c \Lambda_{\text{QCD}}$ with $\Lambda_{\text{QCD}} \simeq 0.2 - 0.3$ GeV, because of N_c quarks collectively moving in the same direction. Remarkably, these baryons are relativistic at relatively low density, $n_B = 1 - 4n_0 \sim \Lambda_{\text{QCD}}^3$, much smaller than naive baryon gas estimates, $n_B \sim 100n_0 \sim P_B^3 \sim (N_c \Lambda_{\text{QCD}})^3$. Including this feature leads to the peak in sound velocity around $n_B = 1 - 4n_0$ [67, 79–84].

Inspired by the work of McLerran and Reddy, one of the authors (T.K.) in this paper introduced a microscopic model of quark-hadron continuity [85]. Although schematic, the model manifestly keeps track of the evolution of the occupation probability for quark states. In dilute baryonic matter, quarks in isolated baryons are superpositions of momentum states from 0 to $\sim \Lambda_{\text{QCD}}$, and each momentum state is occupied with a small probabil-

* torujj@mail.cnu.edu.cn

† suenaga@rcnp.osaka-u.ac.jp

ity. Those quark states at low momenta are progressively occupied as baryon density increases, and at some density those states are fully occupied with the probability one. We call it *quark saturation*. It was found that, with a reasonable size scale for a quark wave function, the quark saturation happens at density considerably less than the density where baryon cores overlap. This may be interpreted as a percolation of low momentum modes, referred as *soft deconfinement* in Ref.[86]. After saturating low momenta, the quark Fermi sea approaches a usual quark matter description. In this description, the peak of sound velocity is triggered by the quark saturation effect, while nuclear interactions tend to smooth out the peak structure. The description contains the above-mentioned quarkyonic matter model as a special case [85].

While QC₂D differs from QCD with three colors in descriptions of baryons, QC₂D can be used to test the quark saturation effects; the baryonic matter in dilute regime is the BEC of diquarks, but such a picture breaks down as the quark occupation probability increases. Also, lattice QC₂D studies found that diquark baryons have hard core repulsions [87]. For these aspects, whether baryons are fermions or bosons may not be crucial, and both cases should induce rapid stiffening associated with the quark saturation. We delineate QC₂D from this point of view¹ to find out concepts which are also useful for QCD.

Another important issue is the effects of interactions. In the context of two solar mass NS, it is important to understand which interactions can stiffen quark matter EoS. To get rough insights, it is useful to start with a simple parametrization of an energy density [58, 61]

$$\varepsilon(n_B) = an_B^{4/3} + bn_B^\alpha, \quad (1)$$

where the first term is from the relativistic kinetic energy for quarks, and the second is from interactions. Taking a derivative to obtain μ_B , using $P = \mu_B n_B - \varepsilon$, and eliminating the coefficient a , one can write the pressure as

$$P = \frac{\varepsilon}{3} + b \left(\alpha - \frac{4}{3} \right) n_B^\alpha. \quad (2)$$

For $\alpha > 4/3$, repulsive ($b > 0$) forces stiffen EoS while attractive forces soften EoS. This trend is seen in low density nuclear physics. Meanwhile, a less known possibility is $\alpha < 4/3$, for which attractive ($b < 0$) forces stiffen EoS. Such attractions with low powers of n_B may happen around the Fermi surface at high density. We argue that EoS becomes very stiff when the bulk part of the quark Fermi sea has effective repulsions but the Fermi surface enjoys the attractive correlations. In QC₂D, the latter is naturally realized as diquark correlations. Taking this schematic description as our baseline, we examine

the effects of interactions using two models. The first is a model based on coherent states of diquarks, and the second is the Nambu-Jona-Lasinio (NJL) model with diquark pairing terms.

This paper is organized as follows. In Sec.II we discuss quarks in baryonic matter and the concept of the occupation probabilities. In Sec.III we compare ideal fermionic and bosonic baryon gases. In Sec.IV we discuss a model of coherent states for diquarks. In Sec.V we study the NJL model. Section VI is devoted to a summary.

II. QUARKS IN BARYONIC MATTER

In this section, we discuss quarks in a dense matter for a general number of colors. We consider the occupation probability, $f_q = f_{q_s^c}$, of a quark state for a given set of color (c), flavor (q), spin (s) in baryonic matter. We postulate the form [85] ($\int_{\mathbf{p}} \equiv \int d^3\mathbf{p}/(2\pi)^3$),

$$f_q(\mathbf{k}; n_B) = \sum_I \int_{\mathbf{K}_B} \mathcal{B}_I(\mathbf{K}_B; n_B) Q_{\text{in}}^{Iq}(\mathbf{k}, \mathbf{K}_B). \quad (3)$$

Here $\mathcal{B}_I(\mathbf{K}_B; n_B)$ is the number of baryons in a quantum state with a momentum \mathbf{K}_B and a baryon spin-flavor (S, S_z, F) , e.g., $\Delta_{S=S_z=3/2}^{++}$. The function Q_{in}^{Iq} is a single quark momentum distribution with a color-spin-flavor species $\mathbf{q} = q_s^c = (u_\uparrow^R, u_\downarrow^R, u_\uparrow^G, \dots)$, specifying the host baryon with a quantum number “ I ”. Since f_q is the probability, it must obey the constraint

$$0 \leq f_q(\mathbf{k}; n_B) \leq 1, \quad (4)$$

which in turn constrains the form of \mathcal{B} [85]. For the normalization of Q_{in}^{Iq} , we set the spatial probability after momentum integration to be 1. Then

$$\int_{\mathbf{k}} Q_{\text{in}}^{Iq}(\mathbf{k}, \mathbf{K}_B) = \langle I | N_{q_s^c} | I \rangle = \frac{1}{N_c} \langle I | N_{q_s} | I \rangle, \quad (5)$$

where $N_{q_s^c}$ is the number operator for a state q_s^c , and $N_{q_s} = \sum_c N_{q_s^c}$ which counts the number of states with a given spin-flavor (q_s).² The total quark number is computed as

$$\begin{aligned} n_q &= \sum_{q_s^c} \int_{\mathbf{k}} f_q(\mathbf{k}; n_B) \\ &= \sum_I \int_{\mathbf{K}_B} \mathcal{B}_I(\mathbf{K}_B; n_B) \sum_{q_s^c} \langle I | N_{q_s^c} | I \rangle \\ &= \sum_I \int_{\mathbf{K}_B} \mathcal{B}_I(\mathbf{K}_B; n_B) \sum_{q_s} \langle I | N_{q_s} | I \rangle, \end{aligned} \quad (7)$$

² For example, at $N_c = 3$, a state $|\Delta_{s_z=3/2}^{++}\rangle = |u_\uparrow^R, u_\uparrow^G, u_\uparrow^B\rangle$ has the matrix element,

$$\langle \Delta_{s_z=3/2}^{++} | N_{u_\uparrow^R} | \Delta_{s_z=3/2}^{++} \rangle = 1 = \frac{\langle \Delta_{s_z=3/2}^{++} | N_{u_\uparrow} | \Delta_{s_z=3/2}^{++} \rangle}{3}, \quad (6)$$

and $\int_{\mathbf{k}} Q_{\text{in}}^{\Delta_{s_z=3/2}^{++} u_\uparrow^R}(\mathbf{k}, \mathbf{K}_B) = 1$ for whatever \mathbf{K}_B .

¹ We note that Ref.[88] also discussed the peak in sound velocity by focusing on the interplay between chiral and diquark condensates. Meanwhile, our scenario is not sensitive to the presence of chiral condensates.

where $\sum_{q_s} = \sum_{q_s^c} / N_c$. We note³

$$\sum_{q_s} \langle I | N_{q_s} | I \rangle = N_c, \quad (9)$$

with which Eq.(7) leads to

$$\frac{n_q}{N_c} = \sum_I \int_{\mathbf{K}_B} \mathcal{B}_I(\mathbf{K}_B; n_B) = \sum_I n_B^I = n_B, \quad (10)$$

as it should.

As the baryon momentum is given by the sum of quark momenta, Q_{in}^{Iq} must satisfy the constraint⁴

$$\mathbf{K}_B = N_c \int_{\mathbf{k}} \mathbf{k} Q_{\text{in}}^{Iq}(\mathbf{k}, \mathbf{K}_B). \quad (11)$$

where we assumed that Q_{in}^{Iq} is the same for all colors and simply multiplied a factor N_c . We further assume that the variance of quark momenta is characterized as

$$\int_{\mathbf{k}} \left(\mathbf{k} - \frac{\mathbf{K}_B}{N_c} \right)^2 Q_{\text{in}}^{Iq}(\mathbf{k}, \mathbf{K}_B) \sim \Lambda_{\text{QCD}}^2, \quad (12)$$

for any \mathbf{K}_B . The scale Λ_{QCD} is about the inverse of a baryon size. This constraint is satisfied by taking the following form,

$$Q_{\text{in}}^{Iq}(\mathbf{k}, \mathbf{K}_B) = Q_{\text{in}}^{Iq} \left(\mathbf{k} - \frac{\mathbf{K}_B}{N_c}, 0 \right). \quad (13)$$

If $|\mathbf{K}_B| \ll N_c \Lambda_{\text{QCD}}$, the term with \mathbf{K}_B can be treated as a small correction of $\sim 1/N_c$.

III. IDEAL BARYON GAS

In this section, we compare fermionic and bosonic baryon gases. The purpose here is to examine to what extent the concepts of QC₂D can be applied for QCD.

A. Fermionic baryon gas

We first consider baryons as fermions. Let us discuss the dilute limit, $n_B \ll \Lambda_{\text{QCD}}^3$, of baryonic matter where baryons are supposed to form an ideal gas. For baryons as fermions, we assumed that the number of spin-flavor states is $g_B = \sum_I 1$, and they are all degenerated. Then

$$\mathcal{B}_I(\mathbf{k}_B; n_B) = \theta(K_B^F - |\mathbf{K}_B|), \quad (14)$$

³ For example, for a proton state $|p\rangle \sim |uud\rangle$ in QCD,

$$\langle p | \sum_{q_s} N_{q_s} | p \rangle = \langle p | (N_{u_\uparrow} + N_{u_\downarrow} + N_{d_\uparrow} + N_{d_\downarrow}) | p \rangle = 3. \quad (8)$$

⁴ As we integrate out $(N_c - 1)$ -quarks in a baryon to get a single quark distribution Q_{in} , the relation, $\mathbf{K}_B = \mathbf{k}_1 + \dots + \mathbf{k}_{N_c}$, is casted onto a constraint on the average momenta, $\mathbf{K}_B = N_c \langle \mathbf{k} \rangle$.

with

$$n_B = \sum_I \frac{(K_B^F)^3}{6\pi^2} \equiv g_B \frac{(K_B^F)^3}{6\pi^2}, \quad (15)$$

where K_B^F is the Fermi momentum of baryons defined through n_B . To compute f_q , the discussions can be simplified by applying the $1/N_c$ expansion to Q_{in}^{Iq} [see Eq.(13)]

$$\begin{aligned} f_q(\mathbf{k}; n_B) &= \sum_I \int_{\mathbf{K}_B} \mathcal{B}_I(\mathbf{K}_B; n_B) \left(Q_{\text{in}}^{Iq}(\mathbf{k}, 0) + \dots \right) \\ &\simeq \frac{n_B}{g_B} \sum_I Q_{\text{in}}^{Iq}(\mathbf{k}, 0), \end{aligned} \quad (16)$$

where \dots are $1/N_c$ corrections. At leading order of $1/N_c$, the function f_q has the \mathbf{k} dependence as Q_{in}^{Iq} , but its magnitude grows linearly with n_B . Recalling the constraint $f_q \leq 1$, the ideal gas picture must be violated for some large n_B . At leading order of $1/N_c$, the saturation of the $\mathbf{k} = 0$ mode in a state q_s takes place when

$$n_B^{\text{id.sat}}|_{\text{LO}} = \left[\frac{1}{g_B} \sum_I Q_{\text{in}}^{Iq}(\mathbf{0}, 0) \right]^{-1}. \quad (17)$$

From the normalization condition, $Q_{\text{in}}^{Iq}(\mathbf{0}, 0) \sim \Lambda_{\text{QCD}}^{-3}$, $n_B^{\text{id.sat}} \sim \Lambda_{\text{QCD}}^3$. Beyond this critical density, the quark Fermi sea with the occupation probability $\simeq 1$ develops.

For simplicity, we estimate the energy density within the quasiparticle picture,

$$\varepsilon(n_B) = \sum_{q_s^c} \int_{\mathbf{k}} E_q(\mathbf{k}) f_q(\mathbf{k}; n_B), \quad (18)$$

where E_q is the single quark energy for states with $\mathbf{q} = q_s^c$. In a dilute limit, the leading order of $1/N_c$ is

$$\begin{aligned} \varepsilon_{\text{dilute}}^{\text{LO}}(n_B) &= \frac{n_B}{g_B} \sum_I \sum_{q_s^c} \int_{\mathbf{k}} E_{q_s^c}(\mathbf{k}) Q_{\text{in}}^{Iq_s^c}(\mathbf{k}, 0) \\ &= \frac{n_B}{g_B} \sum_I M_B^I = n_B M_B, \end{aligned} \quad (19)$$

where in the last step we used the degeneracy $M_B^I = M_B$ for all I . For this energy density the pressure is vanishing

$$P_{\text{dilute}}^{\text{LO}} = n_B^2 \frac{\partial(\varepsilon_{\text{dilute}}^{\text{LO}}/n_B)}{\partial n_B} = 0. \quad (20)$$

The pressure in a dilute limit is vanishing when a constant energy per particle is insensitive to changes in n_B .

This trend of the constant energy per particle must change when the quark saturation effects set in, because the saturated levels require quarks to be added at higher momenta at larger n_B . The energy per particle begins to grow just after the saturation, and the pressure increases rapidly. Especially, if we naively extrapolate an ideal gas expression to the quark saturation point, the n_B dependence of ε/n_B changes discontinuously at the saturation. This leads to an unphysical jump in pressure

[85]. In more realistic treatments, at low density ε/n_B increases more gradually mainly due to baryon-baryon interactions, smearing the unphysical jump.

Throughout this section we have assumed that Q_{in}^{Iq} for quarks in a baryon does not change. In principle, quark states in a baryon should be also affected when the low energy levels are partially filled. This is also expected from meson exchanges between baryons that can be interpreted as quark hopping [86]. We see this sort of modification in the following sections.

B. Bosonic baryon gas

In an ideal gas of elementary bosons, the ground state is the BEC made of bosons at zero momenta. For an ideal or noninteracting gas of composite bosons, we suppose that the BEC description is valid in a dilute regime. Here, we consider only single bosonic baryon in two flavor theories, namely a bosonic baryon made of a color-, flavor-, spin-singlet ud diquarks.⁵ In the BEC the baryon state distribution should be

$$\mathcal{B}^{\text{ideal}}(\mathbf{K}_B; n_B) = n_B (2\pi)^3 \delta(\mathbf{K}_B), \quad (22)$$

which satisfies $n_B = \int_{\mathbf{K}_B} \mathcal{B}^{\text{ideal}}(\mathbf{K}_B; n_B)$. The probability to find, e.g., the state u_{\uparrow}^R state in such a baryon is proportional to $1/2N_f$ where the factor $2N_f$ is from the spin and flavor $N_f = 2$. Substituting Eq.(22) to Eq.(3), we can show

$$f_{\mathbf{q}}^{\text{ideal}}(\mathbf{k}; n_B) \equiv n_B Q_{\text{in}}^{\mathbf{q}}(\mathbf{k}, 0). \quad (23)$$

which is similar to Eq.(16). The condition on a probability, $f_{\mathbf{q}} \leq 1$, is applied as before, so the saturation must take place at some density. For an ideal gas

$$n_B^{\text{id.sat}} = Q_{\text{in}}^{\mathbf{q}}(\mathbf{0}, 0)^{-1} \sim 2N_f \Lambda_{\text{QCD}}^3. \quad (24)$$

The EoS is soft ($P = 0$) before reaching the saturation, and then gets stiffened. This mechanism is the same as in a fermionic baryon gas.

IV. A MODEL OF COHERENT STATES

From this section we begin to take into account interactions. For diquark baryons in QC_2D , relatively simple descriptions of $f_{\mathbf{q}}$ from nuclear to quark matter regime are possible by referring to theories for the BEC-BCS crossover [20, 89, 90]. In this section, we assume the

presence of a hamiltonian which drives the formation of diquark bound states in vacuum. We do not write the hamiltonian explicitly, but assume that the resulting ground state can be described by the coherent states with which the creation and annihilation operators of (composite) bosons have the nonzero expectation values, $\langle d^\dagger \rangle, \langle d \rangle \neq 0$. With these expectation values, the BEC in this section differs from the BEC of noninteracting bosons; the latter is the eigenstate of the number operator $d^\dagger d$ leading to the zero expectation values of boson operators (e.g., $\langle d \rangle = 0$). Hence, intrinsically the BEC in this section is made of interacting bosons. For the stability of uniform Bose gas in dilute regime (no clustering), the boson-boson interactions should be repulsive here. The pressure is nonzero from the dilute regime.

A. Occupation probability

In a dilute regime of interacting bosons, the BEC state can be described as a coherent state (\mathcal{N}, C : constants to be fixed later)

$$|\Phi\rangle \equiv \mathcal{N} \exp [C b_0^\dagger] |0\rangle. \quad (25)$$

We keep this form to the BCS regime. Here $b_{\mathbf{K}_B}^\dagger$ is a creation operator of bosons with \mathbf{K}_B , made of quark creation operators $(a_{\mathbf{k}}^{qs})^\dagger$ as ($N_c = N_f = 2$)

$$b_{\mathbf{K}_B}^\dagger = \frac{\epsilon_{qq'} \epsilon_{cc'}}{\sqrt{N_c N_f}} \int_{\mathbf{k}} \phi_{\mathbf{k}} (a_{\mathbf{k}+\mathbf{K}_B/2}^{q\uparrow})^\dagger (a_{-\mathbf{k}+\mathbf{K}_B/2}^{q'\downarrow})^\dagger. \quad (26)$$

The function $\phi_{\mathbf{k}}$ is a wave function for a relative momentum between two quarks, normalized as $\int_{\mathbf{k}} |\phi_{\mathbf{k}}|^2 = 1$. The form of $\phi_{\mathbf{k}}$ may be density dependent in principle, but we use the same $\phi_{\mathbf{k}}$ during the BEC-BCS crossover. (In this section we neglect hole and antiparticle contributions for simplicity.)

Since the boson operator b_0^\dagger is made of fermions, we can rewrite the coherent state as $(\Phi_{\mathbf{k}} \equiv C \phi_{\mathbf{k}})$

$$\begin{aligned} |\Phi\rangle &= \mathcal{N} \prod_{\mathbf{k}} \exp \left[\Phi_{\mathbf{k}} \frac{\epsilon_{qq'} \epsilon_{cc'}}{2} (a_{\mathbf{k}}^{q\uparrow})^\dagger (a_{-\mathbf{k}}^{q'\downarrow})^\dagger \right] |0\rangle \\ &= \mathcal{N} \prod_{\mathbf{k}} \sum_{n=0}^4 \frac{1}{n!} (\Phi_{\mathbf{k}} A_{\mathbf{k}}^\dagger)^n |0\rangle \end{aligned} \quad (27)$$

where

$$A_{\mathbf{k}}^\dagger = \frac{\epsilon_{qq'} \epsilon_{cc'}}{2} (a_{\mathbf{k}}^{q\uparrow})^\dagger (a_{-\mathbf{k}}^{q'\downarrow})^\dagger. \quad (28)$$

In the product of $A_{\mathbf{k}}^\dagger$, the products of the same fermionic creation operators automatically drop off. For given $(\mathbf{k} \uparrow; -\mathbf{k} \downarrow)$ levels, we have superposition of an empty state $|0; 0\rangle$, a diquark state (e.g., $|u_{\uparrow}^R; d_{\downarrow}^G\rangle$), a tetraquark state (e.g., $|u_{\uparrow}^R u_{\uparrow}^G; d_{\downarrow}^R d_{\downarrow}^G\rangle$), a hexaquark state, (e.g., $|u_{\uparrow}^R u_{\uparrow}^G d_{\uparrow}^R; u_{\downarrow}^G d_{\downarrow}^R d_{\downarrow}^G\rangle$) and an octaquark state, $|u_{\uparrow}^R u_{\uparrow}^G d_{\uparrow}^R d_{\uparrow}^G; u_{\downarrow}^R u_{\downarrow}^G d_{\downarrow}^R d_{\downarrow}^G\rangle$. In the octaquark state all

⁵ The quantum number can be expressed as

$$|B\rangle = \epsilon_{cc'} \epsilon_{qq'} \epsilon_{ss'} \frac{|q_s^c, q_{s'}^{c'}\rangle}{\sqrt{2N_c N_f}}. \quad (21)$$

The normalization factor is included in $Q_{\text{in}}^{\mathbf{q}}$.

color-flavor-spin are filled for a given \mathbf{k} ; states are saturated and no more states are available. For our coherent states, all of these states have finite probabilities; the ground state changes from the BEC to BCS regime smoothly with changes in the weight factor $\Phi_{\mathbf{k}}$.

In a dilute matter, $|\Phi_{\mathbf{k}}| \ll 1$ for all levels and the diquark states are dominant. In a dense matter, there are both dense and dilute levels in momentum space. At low \mathbf{k} , the octaquark states or filled quark Fermi sea are dominant with $|\Phi_{\mathbf{k}}| \gg 1$. But levels at sufficiently high \mathbf{k} have the small weight factors, $|\Phi_{\mathbf{k}}| \ll 1$, leading to a smeared Fermi surface as in the BCS state.

Let us confirm the above-mentioned behaviors. The normalization condition is

$$1 = \langle \Phi | \Phi \rangle = |\mathcal{N}|^2 \prod_{\mathbf{k}} \sum_{n=0}^4 \frac{\mathcal{A}_n |\Phi_{\mathbf{k}}|^{2n}}{(n!)^2}, \quad (29)$$

with the expectation values for each \mathbf{k} ,

$$\mathcal{A}_n \equiv \langle 0 | A_{\mathbf{k}}^n (A_{\mathbf{k}}^\dagger)^n | 0 \rangle. \quad (30)$$

The list is

$$\mathcal{A}_0 = \mathcal{A}_1 = 1, \quad \mathcal{A}_2 = \frac{3}{2}, \quad \mathcal{A}_3 = \mathcal{A}_4 = \frac{9}{4}. \quad (31)$$

Thus, the normalization constant \mathcal{N} is determined for a given set of $\Phi_{\mathbf{k}}$ at various \mathbf{k} . The other constant C is fixed by the condition ($n_q = 2n_B$)

$$n_q = \sum_{q_s^c} \int_{\mathbf{k}} \langle \Phi | n_{\mathbf{k}}^{q_s^c} | \Phi \rangle = \sum_{q_s^c} \int_{\mathbf{k}} f_q(\mathbf{k}; n_B), \quad (32)$$

where $n_{\mathbf{k}}^{q_s^c} = (a_{\mathbf{k}}^{q_s^c})^\dagger a_{\mathbf{k}}^{q_s^c}$. Explicit calculations lead to

$$\begin{aligned} f_q(\mathbf{k}; n_B) &= |\mathcal{N}|^2 \sum_{n=1}^4 \frac{\mathcal{B}_n |\Phi_{\mathbf{k}}|^{2n}}{(n!)^2} \prod_{l \neq \mathbf{k}} \sum_{m=0}^4 \frac{\mathcal{A}_m |\Phi_l|^{2m}}{(m!)^2} \\ &= \sum_{n=1}^4 \frac{\mathcal{B}_n |\Phi_{\mathbf{k}}|^{2n}}{(n!)^2} \bigg/ \sum_{m=0}^4 \frac{\mathcal{A}_m |\Phi_{\mathbf{k}}|^{2m}}{(m!)^2}, \end{aligned} \quad (33)$$

with the expectation values for each \mathbf{k} ,

$$\mathcal{B}_n \equiv \langle 0 | A_{\mathbf{k}}^n n_{\mathbf{k}}^{q_s^c} (A_{\mathbf{k}}^\dagger)^n | 0 \rangle. \quad (34)$$

The list is

$$\mathcal{B}_1 = \frac{1}{4}, \quad \mathcal{B}_2 = \frac{3}{4}, \quad \mathcal{B}_3 = \frac{27}{16}, \quad \mathcal{B}_4 = \frac{9}{4}. \quad (35)$$

The constant C is determined for a given set of the bound state wave functions $\phi_{\mathbf{k}}$ at various \mathbf{k} .

In a dilute matter, $|\Phi_{\mathbf{k}}| \ll 1$ for all \mathbf{k} , and we have

$$n_q = 2n_B \simeq \sum_{q_s^c} \int_{\mathbf{k}} \mathcal{B}_1 |\Phi_{\mathbf{k}}|^2 = 2|C|^2, \quad (36)$$

where we have used $\int_{\mathbf{k}} |\phi_{\mathbf{k}}|^2 = 1$. Now we found $|C|^2 \simeq n_B$ with which

$$f_q(\mathbf{k}; n_B) \simeq \frac{|\phi_{\mathbf{k}}|^2}{4} n_B. \quad (\text{dilute matter}) \quad (37)$$

The occupation probability is proportional to n_B . The factor $1/4 = 1/2N_f$ reflects the probability to find specific spin-flavor quantum numbers (e.g., u_\uparrow^R) from a spin- and flavor-singlet baryon.

Meanwhile, in a dense matter, there are low momentum modes with $|\Phi_{\mathbf{k}}|^2 \gg 1$ and high momentum modes with $|\Phi_{\mathbf{k}}|^2 \ll 1$. For low momentum modes, the expression of f_q is dominated with the $|\Phi_{\mathbf{k}}|^8$ -terms. Here all color-flavor-spin quanta are saturated. Including up to $1/|\Phi_{\mathbf{k}}|^2$ correction, one finds (reminder: $\Phi_{\mathbf{k}} = C\phi_{\mathbf{k}}$)

$$f_q(\mathbf{k}; n_B) \simeq 1 - \frac{4}{|\Phi_{\mathbf{k}}|^2}. \quad (38)$$

Thus f_q approaches 1 from below, as it should.

Finally, we derive the expression for the amplitudes of diquark operators. It is given by

$$\begin{aligned} d_{\mathbf{k}} &\equiv \langle \Phi | A_{\mathbf{k}} | \Phi \rangle = |\mathcal{N}|^2 \prod_{\mathbf{k}} \Phi_{\mathbf{k}} \sum_{n=1}^4 \frac{\mathcal{A}_n |\Phi_{\mathbf{k}}|^{2(n-1)}}{n!(n-1)!} \\ &= \Phi_{\mathbf{k}} \sum_{n=1}^4 \frac{\mathcal{A}_n |\Phi_{\mathbf{k}}|^{2(n-1)}}{n!(n-1)!} \bigg/ \sum_{m=0}^4 \frac{\mathcal{A}_m |\Phi_{\mathbf{k}}|^{2m}}{(m!)^2}. \end{aligned} \quad (39)$$

Here $d_{\mathbf{k}}$ is a dimensionless quantity. Diquark condensates are obtained after integrating $d_{\mathbf{k}}$ over the phase space, $\int_{\mathbf{k}}$.

Now, we try to gain the analytic insights. For dilute levels ($|\Phi_{\mathbf{k}}|^2 \ll 1$),

$$d_{\mathbf{k}} \simeq \Phi_{\mathbf{k}}. \quad (40)$$

In particular, if all levels are dilute, we may further use $|C|^2 \simeq n_B$ (Eq.(36)) to get $d_{\mathbf{k}} \simeq \sqrt{n_B} \phi_{\mathbf{k}}$. On the other hand, for dense levels ($|\Phi_{\mathbf{k}}|^2 \gg 1$),

$$d_{\mathbf{k}} \simeq 4 \frac{\Phi_{\mathbf{k}}}{|\Phi_{\mathbf{k}}|^2} \simeq \Phi_{\mathbf{k}} [1 - f_q(\mathbf{k}; n_B)]. \quad (41)$$

In the last step we used Eq.(38). Thus, the diquark amplitudes are small for occupied levels.

B. A model of gaussian wave functions

We now take a specific spatial wave function for composite bosons, and use them together with the formulas in Sec.IV A. We postulate the form

$$|\Phi_{\mathbf{k}}|^2 = |C\phi_{\mathbf{k}}|^2 = |C|^2 \left(\frac{2\sqrt{\pi}}{\Lambda} \right)^3 e^{-\mathbf{k}^2/\Lambda^2}, \quad (42)$$

where Λ characterizes the size of diquarks. Taking the Fourier transform of $\phi_{\mathbf{k}}$ and then squaring it, we obtain the probability of two quarks to have a relative distance $|\mathbf{r}|$,

$$|\phi_{\mathbf{r}}|^2 = \text{const.} \times e^{-\Lambda^2 \mathbf{r}^2}, \quad (43)$$

from which one can calculate the average distance of two quarks in a baryon as

$$\langle \mathbf{r}^2 \rangle = 3\Lambda^{-2} \frac{\int d\mathbf{x} x^2 e^{-x^2}}{\int d\mathbf{x} e^{-x^2}} = \frac{3}{2\Lambda^2}. \quad (44)$$

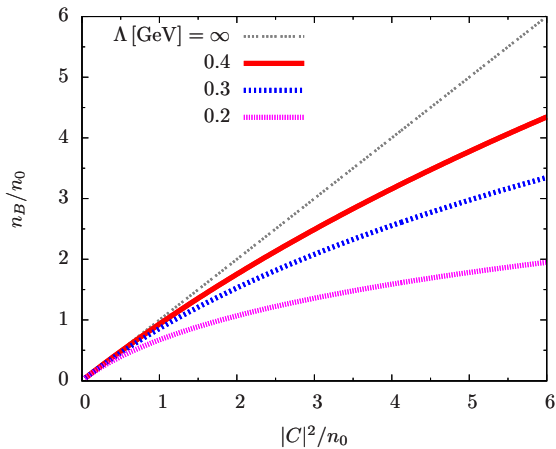


FIG. 1. $|C|^2$ vs n_B , each normalized by $n_0 = 0.16 \text{ fm}^{-3}$. The value of $|C|^2$ corresponds to n_B in the ideal Bose gas limit in which the composite nature is neglected or Λ is taken to be infinity.

Thus, the average distance from the center is

$$R \equiv \frac{\sqrt{\langle r^2 \rangle}}{2} \simeq 0.612 \text{ fm} \times \left(\frac{0.197 \text{ GeV}}{\Lambda} \right). \quad (45)$$

This defines our baryon core radius in this paper. We estimate the density where baryon cores overlap as

$$n_B^{\text{overlap}} \equiv \frac{1}{4\pi R^3/3} \simeq 1.04 \text{ fm}^{-3} \left(\frac{\Lambda}{0.197 \text{ GeV}} \right)^3. \quad (46)$$

For $\Lambda \simeq 0.2 \text{ GeV}$, we find $n_B^{\text{overlap}} \simeq 6.5n_0$. It is also convenient to evaluate the density for the quark saturation at $\mathbf{k} = 0$. Our measure is [see Eqs.(24) or (37) for $f_q(\mathbf{k} = 0; n_B)$]

$$n_B^{\text{id.sat}} = 2N_f \left(\frac{\Lambda}{2\sqrt{\pi}} \right)^3 \simeq 0.09 \text{ fm}^{-3} \left(\frac{\Lambda}{0.197 \text{ GeV}} \right)^3 \quad (47)$$

For $\Lambda \simeq 0.2 \text{ GeV}$, we find $n_B^{\text{id.sat}} \simeq 0.56n_0$. This density is much smaller than that for baryons to overlap.

Now, we first examine to what extent the ideal Bose gas expressions in Sec.III B are valid. We recall that, in the ideal gas limit, the parameter $|C|^2$ equals to n_B [see Eq.(36)]. This equality is violated when the composite natures of baryons become important. Shown in Fig.1 is the $|C|^2$ vs n_B , each normalized by $n_0 = 0.16 \text{ fm}^{-3}$. The relations are naturally sensitive to Λ or the baryon size. The limit $\Lambda \rightarrow \infty$ corresponds to the point particle limit, and $|C|^2 = n_B$. This simple relation does not hold for a smaller Λ ; boson-boson interactions⁶ as well as the composite nature of bosons make n_B less than $|C|^2$. Remarkably, these effects are substantial at density much

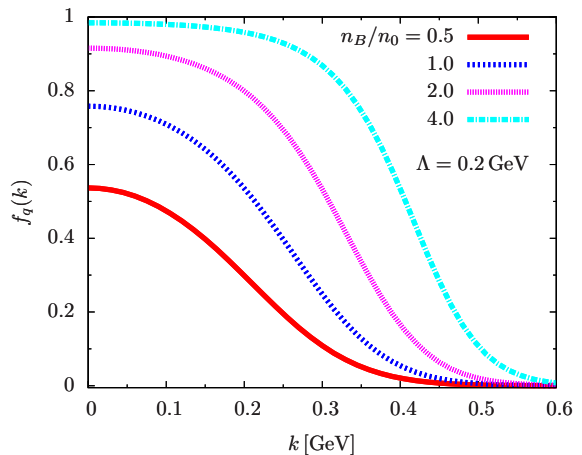


FIG. 2. The occupation probability $f_q(k)$ as a function of momentum k . The cases $n_B/n_0 = 0.5, 1.0, 2.0,$ and 4.0 cases are shown.

smaller than n_B^{overlap} and $n_B^{\text{id.sat}}$. For instance, for $\Lambda = 0.2 \text{ GeV}$, the deviation from the ideal gas limit is significant around $n_B \simeq 0.5n_0$. The coherent state is substantially different from the ideal Bose gas limit already at rather low density.

Next, we examine the occupation probability of quark states, see Fig.2 for the $\Lambda = 0.2 \text{ GeV}$ case. One can readily see that $\sim 50\%$ of the $k = 0$ states are occupied at $n_B = 0.5n_0$, and $\sim 100\%$ at $n_B = 4n_0$. At $n_B = 0.5n_0$, one can see the Gaussian shape, but at higher density the shape is deformed. The growth rate of the occupation probability becomes smaller for low momentum states, and then states with higher momenta grow more substantially instead. To see this trend more clearly, we examine the ratio

$$f_q(k)/f_q^{\text{ideal}}(k), \quad (48)$$

where f_q^{ideal} is estimated by the expression of Eq.(37). The result is shown in Fig.3. If we neglect the composite nature of baryons, the ratio remains 1 for all momenta. As density increases, the low momentum part of the ratio drops as the quark Pauli blocking effect tempers the growth in f_q , and instead the higher momentum part in f_q is increased more than in f_q^{ideal} , leaving substantial enhancement in the ratio f_q/f_q^{ideal} at high momenta. At $n_B \simeq 0.5n_0$, the occupation probability is considerably modified from the ideal gas limit.

Finally we examine a diquark amplitude $d_{\mathbf{k}}$ which is dimensionless (Fig.4). From Eqs.(40) and (41), its size is determined by the product of $\Phi_{\mathbf{k}}$ and $1 - f_q$. For a large k , $\Phi_{\mathbf{k}}$ becomes small but $1 - f_q \simeq 1$. For a small k , $\Phi_{\mathbf{k}}$ is large but $1 - f_q$ can be small at large n_B . Hence, $d_{\mathbf{k}}$ should take the maximum near the Fermi surface, as clearly seen in Fig.4.

⁶ The effects of interactions are implicitly included by saying that the ground state is given by a coherent state with nonzero diquark amplitudes.

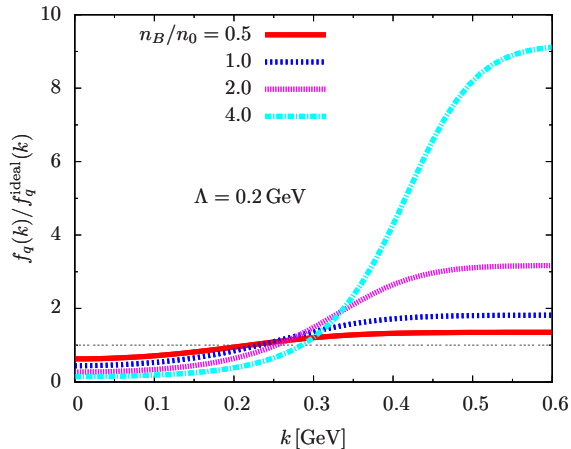


FIG. 3. The $f_q(k)/f_q^{\text{ideal}}(k)$ ratio for various n_B . The ratio measures how the quark Fermi sea differs from naive extrapolation of the ideal gas estimate.

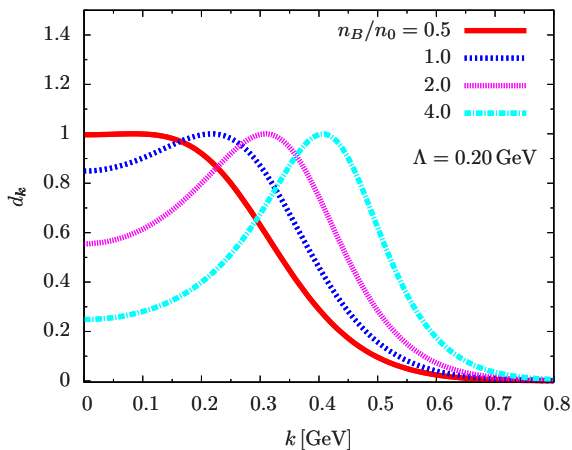


FIG. 4. The (dimensionless) diquark amplitude d_k as a function of momentum k . The cases $n_B/n_0 = 0.5, 1.0, 2.0,$ and 4.0 cases are shown.

C. A model of single quark energy for EoS

So far we have assumed the presence of a hamiltonian which favors the coherent states as ground states at given density, but have not discussed the energies explicitly. Here, we assume some form of average single particle energies and calculate the EoS within a quasiparticle picture. We postulate the parametrization ($\beta > 0$)

$$E_{\text{CQM}}(\mathbf{k}) = \sqrt{M_q^2 + \mathbf{k}^2} - C_A + C_S [f_q(k)]^\beta, \quad (49)$$

where M_q is the constituent quark mass, and C_A and C_S are two-body semishort range correlations where A and S stand for color-singlet (antisymmetric) and triplet

(symmetric) channels⁷. In a baryon or in a dilute matter, any two quarks are in the color-antisymmetric combination. Meanwhile, color-symmetric interactions occur only when two baryons are close and quarks from different baryons interact. These pictures are reflected in our parametrization. In average, a quark has the energy reduction by C_A , while C_S is suppressed by factors $[f_q(k)]^\beta \ll 1$. At a large density, quarks have more chance to interact with quarks in a color symmetric channel. For occupied levels with $f_q(k) \sim 1$, the repulsive energy grows up.

With this single particle energy, the baryon mass is computed as the sum of average quark energy,

$$\begin{aligned} M_B &= N_c \int_{\mathbf{k}} E_{\text{CQM}}(\mathbf{k}) |\phi_{\mathbf{k}}|^2 \\ &= N_c \left(\int_{\mathbf{k}} |\phi_{\mathbf{k}}|^2 \sqrt{M_q^2 + \mathbf{k}^2} - C_A \right). \end{aligned} \quad (50)$$

Below we set $M_q = 0.3$ GeV and $\Lambda = 0.2$ GeV. For $C_A = 0$, the baryon mass is $M_B \simeq 0.77$ GeV with 0.60 GeV from the quark rest masses and 0.17 GeV from the quark kinetic energy. We examine $C_A = 0.085, 0.185,$ and 0.285 GeV which give $M_B = 0.6, 0.4,$ and 0.2 GeV, respectively.

For computations of EoS, we first set $C_S = 0$. We use the measures

$$\varepsilon^{\text{id.sat}} \equiv M_B n_B^{\text{id.sat}}, \quad (51)$$

to estimate the energy density which the ideal gas picture would yield at the density of quark saturation. For C_A 's to yield $M_B = 0.6, 0.4,$ and 0.2 GeV, the corresponding $\varepsilon^{\text{id.sat}}$ are $0.054, 0.036,$ and 0.018 GeVfm⁻³, respectively. The corresponding pressure is zero because ε/n_B is constant with respect to changes in n_B .

For these sets of parameters, the ε vs P is shown in Fig.5. First of all, all these curves suggest that the pressure at $n_B = n_B^{\text{id.sat}}$ is not close to the ideal Bose gas limit, $P = 0$. Rather, the results of the coherent state smoothly approach the quark matter behaviors with the slope $dP/d\varepsilon = c_s^2$ close to $1/3$. In particular, the speed of sound is already substantial before reaching $n_B^{\text{id.sat}}$, and no peaks are found (Fig.6). We note EoS is stiffer for a larger C_A . This is because (with a given kinetic energy) a quark in attractive correlations can appear with the smaller energies.

Now, we turn on interactions in the color-symmetric channels, C_S , for $C_A = 0.285$ GeV ($M_B = 0.2$ GeV). We set $C_S = C_A$ for simplicity and vary the powers β [see

⁷ A more reasonable modeling should also distinguish spin-flavor channels. For a scalar diquark as discussed here, both color-electric and magnetic interactions act as attractions between two quarks, as in the case for pions in constituent quark models [91]. In this context, the values of C_A should be interpreted as the sum of these two interactions.

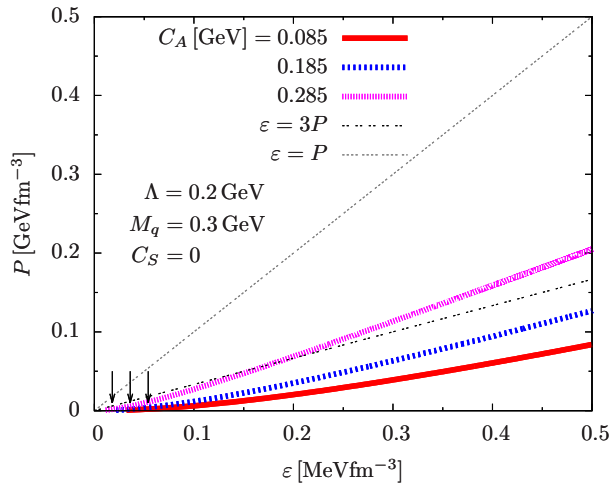


FIG. 5. ϵ vs P for various C_A . We set $\Lambda = 0.2$ GeV, $M_q = 0.3$ GeV, and $C_S = 0$. The arrows indicate the location of $\epsilon_B^{\text{id.sat}} = M_B n_B^{\text{id.sat}}$. For $\Lambda = 0.2$ GeV, the ideal gas picture should have the quark saturation at $n_B^{\text{id.sat}} \simeq 0.56n_0$.

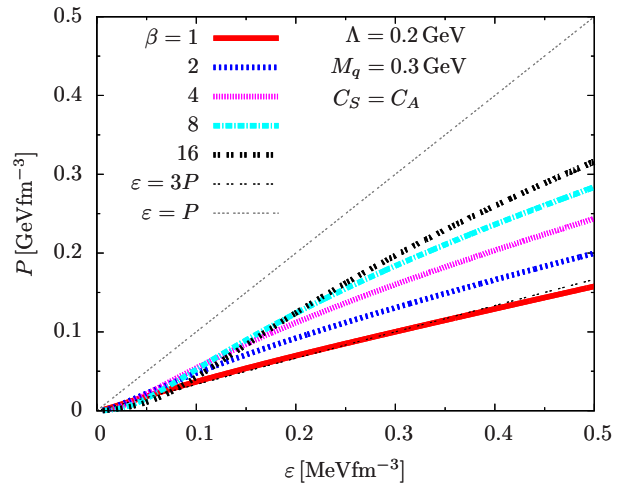


FIG. 7. ϵ vs P for various C_A . We set $\Lambda = 0.2$ GeV, $M_q = 0.3$ GeV, and $C_S = 0$. For $\Lambda = 0.2$ GeV, the ideal gas picture should have the quark saturation at $\epsilon \simeq 0.018$ GeVfm $^{-3}$ ($n_B^{\text{id.sat}} = 0.56n_0$).

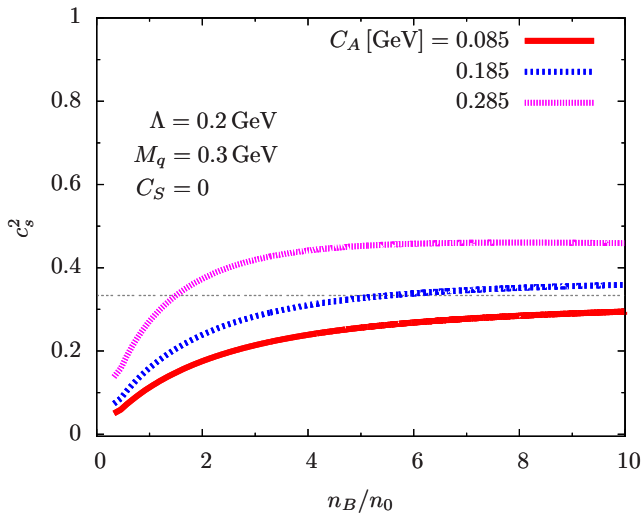


FIG. 6. The square of sound velocity c_s^2 as a function of n_B . We set $\Lambda = 0.2$ GeV, $M_q = 0.3$ GeV, and $C_S = 0$. The conformal value $c_s^2 = 1/3$ is also shown as a guide.

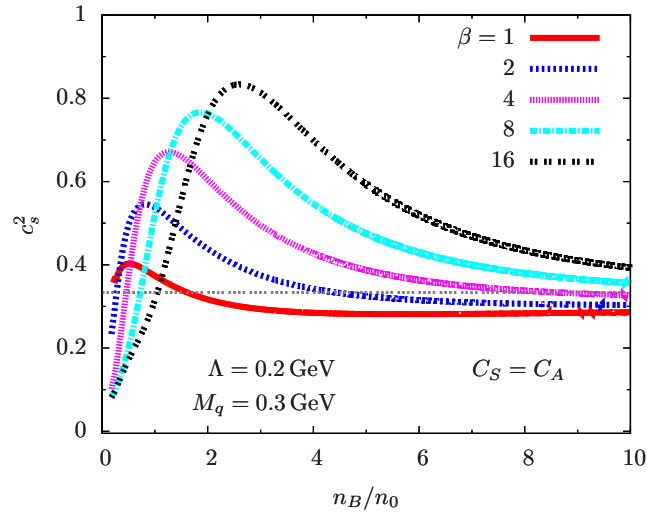


FIG. 8. The square of sound velocity c_s^2 as a function of n_B . We set $\Lambda = 0.2$ GeV, $M_q = 0.3$ GeV, and $C_S = C_A$. The conformal value $c_s^2 = 1/3$ is also shown as a guide.

Eq.(49)]. The interaction part of a quark energy behaves as

$$-C_A + C_S [f_q(k)]^\beta \sim -C_A (1 - [f_q(k)]^\beta). \quad (52)$$

For a larger β , the contrast between the filled and empty levels is sharper. Also, the effect of the repulsion is more suppressed ($[f_q(k)]^\beta \ll 1$) at low density.

Shown in Fig.7 is ϵ vs P , and, in Fig.8, n_B/n_0 vs c_s^2 . The color-symmetric repulsion with $\beta \geq 1$ stiffens the EoS. For a smaller β , the stiffening takes place at low density. For a larger β , the repulsion sets in only when f_q is very close to 1. The location of stiffening can be most clearly identified by peaks in c_s^2 (Fig.8). Next, we examine why a larger β leads to a stiffer EoS at high den-

sity. For modes with $f_q(k) \simeq 1$, the powers β no longer matter. On the other hand, the correlations near the Fermi surface are sensitive to how much the repulsion is suppressed by the factor $[f_q(k)]^\beta$. For $C_A \gg C_S [f_q(k)]^\beta$, the attractive correlations dominate over the repulsive one, and the attractive correlations near the Fermi surface stiffens EoS, as advertised in Eq.(2).

V. THE NJL MODEL

In this section, we discuss stiffening of matter in the two color and two flavor NJL model [92]. The model can describe the chiral symmetry breaking/restoration, di-

quark condensations, the structural changes in hadrons, and so on [5, 7–11]. Although the model does not include confining effects, baryons appear as composite particles whose masses in a dilute limit equal to the pion mass. Thus, we expect that the stiffening mechanism in the previous sections has some validity. We further elucidate various dynamical effects.

We consider light doublet fields $q = (u, d)^T$. Our model Lagrangian is

$$\mathcal{L}_{\text{NJL}} = \bar{q}(i\cancel{\partial} - m + \mu\gamma_0)q + \mathcal{L}_4, \quad (53)$$

where $m = m_u = m_d$ is the current quark masses, and \mathcal{L}_4 describes the chiral and diquark correlations among (u, d) quarks,

$$\mathcal{L}_4 = G [(\bar{q}\tau_a q)^2 + (\bar{q}i\gamma_5\tau_a q)^2] + H [|\bar{q}i\gamma_5\tau_2\sigma_2 q_C|^2 + |\bar{q}\tau_2\sigma_2 q_C|^2]. \quad (54)$$

This part of the Lagrangian is symmetric under $U(N_f)_L \otimes U(N_f)_R \otimes SU(N_c)$ transformations. To check the symmetry for the last diquark terms, it is convenient to rewrite

$$|\bar{q}i\gamma_5\tau_2\sigma_2 q_C|^2 + |\bar{q}\tau_2\sigma_2 q_C|^2 = 2|\bar{q}_L\tau_2\sigma_2 q_L^C|^2 + 2|\bar{q}_R\tau_2\sigma_2 q_R^C|^2. \quad (55)$$

In the last expression, each term is singlet in the $U(N_f)_L \otimes U(N_f)_R \otimes SU(N_c)$ group. Note that the $(qq)_L(\bar{q}\bar{q})_R$ type cross terms are canceled so that the Lagrangian is $U(1)_A$ symmetric. In this work we neglect the determinant interaction which breaks the $U(1)_A$ symmetry [8, 92].

A. Mean field thermodynamics

In the mean field approximation,

$$\mathcal{L}_4^{\text{MF}} = 4G\sigma_f(\bar{q}q)_f - 2G\sigma_f^2 - Hd^\dagger(\bar{q}_C\gamma_5\tau_2\sigma_2 q) + Hd(\bar{q}\gamma_5\tau_2\sigma_2 q_C) - H|d|^2 \quad (56)$$

where the mean fields are given by

$$\sigma_f = \langle(\bar{q}q)_f\rangle, \quad d = \langle\bar{q}_C\gamma_5\tau_2\sigma_2 q\rangle. \quad (57)$$

The effective mass and diquark gap are given by

$$M_f = m_f - 4G\sigma_f, \quad \Delta = -2Hd. \quad (58)$$

Below we assume $M = M_u = M_d$. Using the Nambu-Gor'kov bases, $\Psi = (q, q_c)/\sqrt{2}$, the mean-field Lagrangian can be written as

$$\mathcal{L}_{\text{MF}} = \bar{\Psi}(-iS)\Psi - 2G\sigma_f^2 - H|d|^2, \quad (59)$$

where S is the Nambu-Gor'kov propagator,

$$-iS^{-1} = \begin{pmatrix} i\cancel{\partial} - \hat{M} + \mu\gamma_0 & \Delta\gamma^5\tau_2\sigma_2 \\ -\Delta^*\gamma^5\tau_2\sigma_2 & i\cancel{\partial} - \hat{M} - \mu\gamma_0 \end{pmatrix}, \quad (60)$$

The mean field thermodynamic potential is (T : temperature, μ : quark chemical potential)

$$\Omega_{\text{MF}} = N_c N_f \sum_{\xi=p,a} \int_{\mathbf{k}} \left[-\epsilon_{\mathbf{k}}^\xi - 2T \ln \left(1 + e^{-\epsilon_{\mathbf{k}}^\xi/T} \right) \right] + 2G\sigma_f^2 + H|d|^2. \quad (61)$$

with the quasiparticle energies

$$\epsilon_{\mathbf{k}}^\xi = \sqrt{(E_{\mathbf{k}} - \eta_\xi\mu)^2 + |\Delta|^2}, \quad (62)$$

where we introduced $\eta_p = +1$ and $\eta_a = -1$ and $E_{\mathbf{k}} = \sqrt{\mathbf{k}^2 + M^2}$. As measures of occupation probability, it is common to use the functions

$$|u_\xi(\mathbf{k})|^2 = \frac{1}{2} \left(1 + \frac{E_{\mathbf{k}} - \eta_\xi\mu}{\epsilon_{\mathbf{k}}^\xi} \right), \quad |v_\xi(\mathbf{k})|^2 = \frac{1}{2} \left(1 - \frac{E_{\mathbf{k}} - \eta_\xi\mu}{\epsilon_{\mathbf{k}}^\xi} \right), \quad (63)$$

which satisfy

$$|u_\xi(\mathbf{k})|^2 + |v_\xi(\mathbf{k})|^2 = 1, \quad u_\xi(\mathbf{k})v_\xi(\mathbf{k}) = \frac{\Delta}{2\epsilon_\xi(\mathbf{k})}. \quad (64)$$

The baryon number density $n_B^{\text{MF}} = n_q^{\text{MF}}/N_c$ with $n_q^{\text{MF}} = -\partial\Omega_{\text{MF}}/\partial\mu$ is

$$n_q^{\text{MF}} = 2N_f \int_{\mathbf{k}} (f_p^{\text{MF}}(\mathbf{k}) - f_a^{\text{MF}}(\mathbf{k})), \quad (65)$$

where $f_{p,a}^{\text{MF}}$ is the quark and antiquark occupation probabilities,

$$f_\xi^{\text{MF}}(\mathbf{k}) \equiv |v_\xi(\mathbf{k})|^2(1 - 2n_{\mathbf{k}}^\xi) + n_{\mathbf{k}}^\xi, \quad (66)$$

with the Fermi-Dirac distribution function

$$n_{\mathbf{k}}^\xi = \frac{1}{1 + e^{\epsilon_{\mathbf{k}}^\xi/T}}. \quad (67)$$

In the zero temperature limit, $n_{\mathbf{k}}^\xi \rightarrow 0$.

B. Numerical analyses

We now numerically examine the mean field EoS. We use the following set of parameters:

$$\Lambda = 1.0 \text{ GeV}, \quad G\Lambda^2 = 2.8, \quad m_q = 5 \text{ MeV}, \quad (68)$$

which yield the vacuum pion mass $m_\pi \simeq 0.17 \text{ GeV}$ and the vacuum constituent quark mass $M \simeq 0.31 \text{ GeV}$. We restrict ourselves to the $T = 0$ case. We first present the bulk results for EoS and then analyze the microscopic aspects.

Shown in Fig.9 are the Dirac mass (M), diquark gap (Δ), and normalized baryon number density (n_B/n_0) where $n_0 = 0.16 \text{ fm}^{-3}$ for $H = G$ (bold lines) and $H = 0$ (thin lines). The onset of baryon density is sensitive

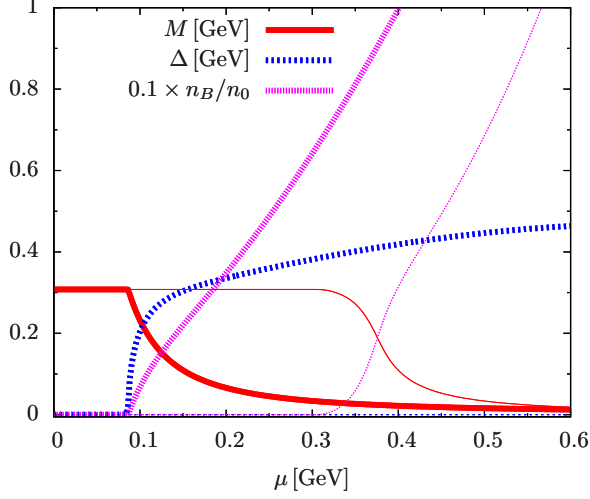


FIG. 9. The Dirac mass (M), diquark gap (Δ), and normalized baryon number density n_B/n_0 with $n_0 = 0.16 \text{ fm}^{-3}$. The thin lines are the results for $H = 0$ with which $\Delta = 0$.

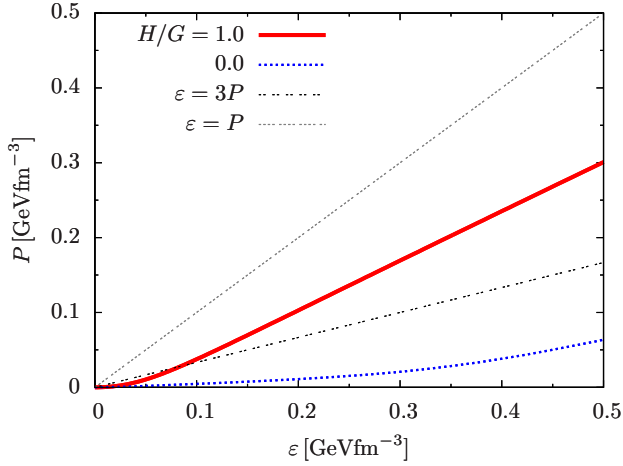


FIG. 10. The ε vs P for $H/G = 1.0$ and 0.0 . The results for $\varepsilon = 3P$ and P are also shown as guide lines.

to the parameter H . For $H = G$, the baryon density is brought by the diquark baryon with the mass m_π , and the corresponding quark chemical potential is $\mu_q = \mu_B/2 = m_\pi/2$. For $H = 0$, there are no composite baryons, and the baryon density becomes nonzero at $\mu_q = M$.

Shown in Figs.10 is ε vs P , which measures the stiffness of EoS. As guidelines, we also show EoS with $\varepsilon = 3P$ and $\varepsilon = P$ for which $c_s^2 = 1/3$ and 1, respectively. For $H = G$, the pressure is substantial at relatively small ε . This is in sharp contrast with the $H = 0$ case where the pressure develops very slowly with increasing ε . With diquark attractions, quarks can appear with small energies at a given pressure, as discussed in Sec.IV C.

The rapid stiffening can be characterized by the behavior of the sound velocity, n_B/n_0 vs c_s^2 , as shown in Fig.11. The sound velocity for $H = G$ exceeds the conformal limit at relatively low density, $n_B/n_0 \simeq 1.2$, reaches

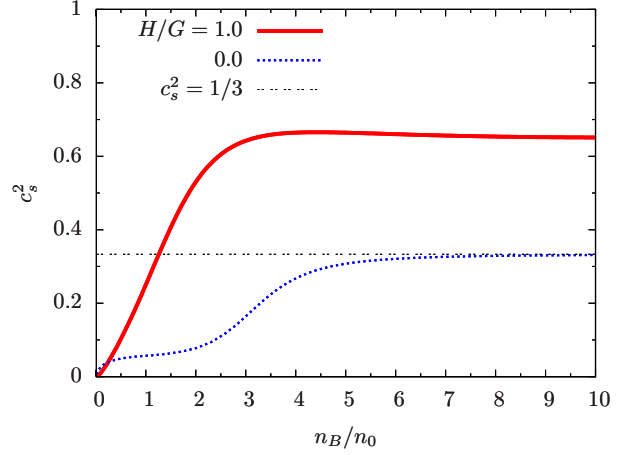


FIG. 11. The n_B/n_0 vs c_s^2 for $H/G = 1.0$ and 0.0 .

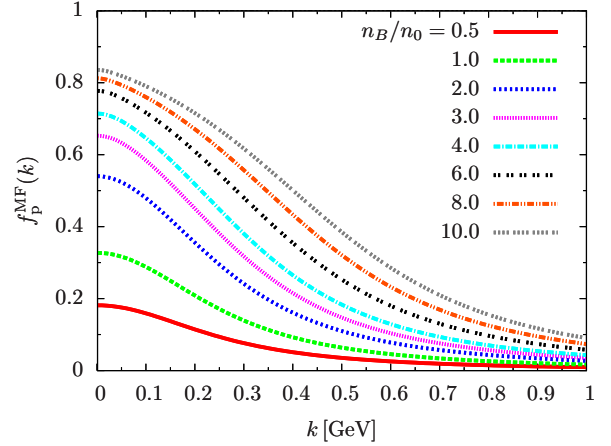


FIG. 12. The occupation probability of particle states, $f_p^{\text{MF}}(k)$, for various n_B/n_0 .

the maximum at $n_B/n_0 \sim 4$, and gradually decreases. In contrast, for $H = 0$ the sound velocity very slowly grows with density and approach the conformal value $c_s^2 = 1/3$ from below.

As we have seen in our model of coherent states, the states with high momenta are occupied substantially even before the saturation of low momentum states is completed. The behavior of $f_p^{\text{MF}}(k)$ is shown in Fig.12. For example, from $n_B/n_0 = 0.5$ to 1.0 , the occupation probability of the $k = 0$ state already does not scale as $\sim n_B$. With increasing n_B , the states at high momenta are occupied more rapidly than in the ideal gas case, and accordingly ε/n_B and hence P grow.

Finally we take a look at the occupation probability for antiparticle states. In the NJL model, the gap Δ is common for particle and antiparticle states. As a consequence the impacts of Δ on antiparticle states are not small. The occupation probability initially increases as Δ does, but at $n_B/n_0 \simeq 3$ the antiparticle suppression by large μ eventually dominates over the effects from Δ .

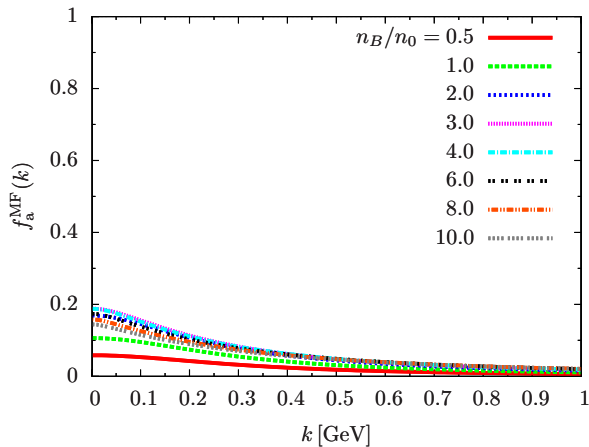


FIG. 13. The occupation probability of antiparticle states, $f_a^{\text{MF}}(k)$, for various n_B/n_0 .

VI. SUMMARY

We have discussed stiffening of matter in QC_2D within the coherent state model and NJL model. In both models diquark baryons appear as composite particles. A dense matter of composite objects observes quarks as their constituents, and is subject to the quark saturation effects that stiffen EoS. Here, we summarize our findings, their implications for QCD, and future works.

(i) The quark saturation effects affect diquark baryons at density significantly lower than the overlapping density of baryon cores. For diquarks with the radii ~ 0.6 fm, the saturation effects are substantial already at $n_B \sim 0.5 - 1n_0$. In three color QCD, this density range is regarded as the territory of conventional nuclear physics where the matter properties depend on intricate balance among various nuclear forces. It is interesting to ask whether using quark descriptions simplifies some part of the nuclear matter descriptions at $n_B \sim n_0$.

(ii) In the coherent state model, a baryonic matter quickly gets stiffened and approaches the quark matter regime at low density. With this small disparity between baryonic and quark matter regimes, the quark saturation effects alone lead to only a rather mild peak in the sound velocity. The peak becomes more prominent when baryonic matter stays soft before the quark saturation effects set in (Fig.14). In QCD, nuclear matter at $n_B \simeq n_0$ is soft, and in this quantitative aspect the three color case somewhat differs from baryonic matter in QC_2D .

(iii) In a dilute regime, attractive correlations inside a baryon, which reduces the baryon mass, stiffens EoS. This is simply because the energy density tends to be smaller for a smaller baryon mass. In terms of the parameterized EoS in Eq.(1) of Sec.I, here we are considering the case with $b < 0$ and $\alpha = 1$. The same feature was also found in the three color case [85].

(iv) In a dense regime, attractive correlations near the Fermi surface stiffens EoS. This has been discussed in models for QCD [58–62], and we also reassure its impact

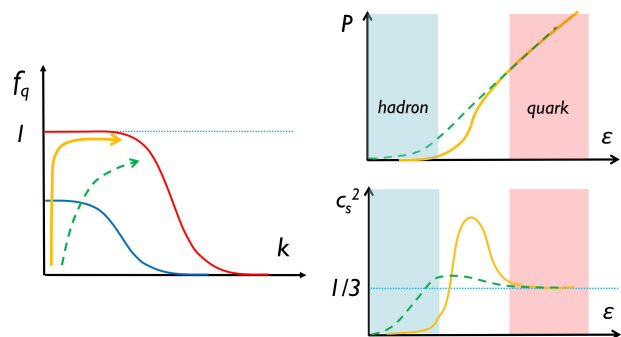


FIG. 14. The relations among $f_q(k)$ and EoS. When f_q evolves as in an ideal baryon gas picture, then the quark saturation radically stiffens EoS and makes a peak in the sound velocity $c_s^2 = dP/d\varepsilon$. If the baryon gas picture breaks down at lower density, stiffening mildly occurs from low density and the peak structure is modest or absent.

in QC_2D .

(v) The best combination to stiffen EoS is to have attractive correlations near the Fermi surface but repulsive correlations in the bulk part of the Fermi sea, as demonstrated in this work and also in the three color studies [85]. This surface-bulk disparity on the sign of interactions may be explained by perturbative gluon exchanges; they lead to the color electric interactions, which overall reduces the energy of color-singlet states, and magnetic interactions, which reduces the energy for color- and spin-singlet states [91]. In a dilute regime, a matter is dominated by states in attractive correlations, but in a denser regime repulsive channels are also unavoidable. This channel dependence leads to the above-mentioned disparity.

We believe that many aspects discussed in this paper, except the quantitative details of baryonic matter, are common for QC_2D and QCD. This work is largely based on effective models and focus on the transition regime. Meanwhile, it is also interesting to study the high density regime where weak coupling methods may be applicable [93–102]. There QC_2D and QCD may be similar and it may be possible to derive a constraint on QCD EoS from the high density side.

Finally, we close this paper by mentioning a significant advantage to use a single framework from baryonic to quark matter regimes. While implicit, our descriptions did not allow the liberty to add a bag constant by hand. In a single model, there are no questions about the *normalizations of EoS* for baryonic and quark matter, or no subtleties about the subtraction of the vacuum or Dirac sea contributions [103]. In QC_2D , a single model description was possible as baryons are just two particles. The same program should be carried out for QCD by handling three particle correlations from nuclear to quark matter regime. Attempts toward this goal are in progress.

ACKNOWLEDGMENT

T. K. thanks Dr. Hatsuda for his questions on the sound velocity in the BEC-BCS crossover, Dr. Yasu-

take for discussions during a NS workshop at RIKEN, and Drs. Tachibana and Hidaka for discussions during a workshop on the thermal field theory. T. K. is supported by NSFC grant No. 11875144.

-
- [1] J. B. Kogut, M. A. Stephanov, and D. Toublan, On two color QCD with baryon chemical potential, *Phys. Lett. B* **464**, 183 (1999), [arXiv:hep-ph/9906346](#).
- [2] J. B. Kogut, M. A. Stephanov, D. Toublan, J. J. M. Verbaarschot, and A. Zhitnitsky, QCD - like theories at finite baryon density, *Nucl. Phys. B* **582**, 477 (2000), [arXiv:hep-ph/0001171](#).
- [3] K. Splittorff, D. T. Son, and M. A. Stephanov, QCD - like theories at finite baryon and isospin density, *Phys. Rev. D* **64**, 016003 (2001), [arXiv:hep-ph/0012274](#).
- [4] T. Kanazawa, T. Wettig, and N. Yamamoto, Chiral Lagrangian and spectral sum rules for dense two-color QCD, *JHEP* **08**, 003, [arXiv:0906.3579 \[hep-ph\]](#).
- [5] G.-f. Sun, L. He, and P. Zhuang, BEC-BCS crossover in the Nambu-Jona-Lasinio model of QCD, *Phys. Rev. D* **75**, 096004 (2007), [arXiv:hep-ph/0703159](#).
- [6] L. He, Nambu-Jona-Lasinio model description of weakly interacting Bose condensate and BEC-BCS crossover in dense QCD-like theories, *Phys. Rev. D* **82**, 096003 (2010), [arXiv:1007.1920 \[hep-ph\]](#).
- [7] C. Ratti and W. Weise, Thermodynamics of two-colour QCD and the Nambu Jona-Lasinio model, *Phys. Rev. D* **70**, 054013 (2004), [arXiv:hep-ph/0406159](#).
- [8] T. Brauner, K. Fukushima, and Y. Hidaka, Two-color quark matter: U(1)(A) restoration, superfluidity, and quarkyonic phase, *Phys. Rev. D* **80**, 074035 (2009), [Erratum: *Phys.Rev.D* **81**, 119904 (2010)], [arXiv:0907.4905 \[hep-ph\]](#).
- [9] J. O. Andersen and T. Brauner, Phase diagram of two-color quark matter at nonzero baryon and isospin density, *Phys. Rev. D* **81**, 096004 (2010), [arXiv:1001.5168 \[hep-ph\]](#).
- [10] J. O. Andersen, T. Brauner, and W. Naylor, Confronting effective models for deconfinement in dense quark matter with lattice data, *Phys. Rev. D* **92**, 114504 (2015), [arXiv:1505.05925 \[hep-ph\]](#).
- [11] S. Imai, H. Toki, and W. Weise, Quark-Hadron Matter at Finite Temperature and Density in a Two-Color PNJL model, *Nucl. Phys. A* **913**, 71 (2013), [arXiv:1210.1307 \[nucl-th\]](#).
- [12] D. Suenaga and T. Kojo, Delineating chiral separation effect in two-color dense QCD, *Phys. Rev. D* **104**, 034038 (2021), [arXiv:2105.10538 \[hep-ph\]](#).
- [13] T. Kojo and D. Suenaga, Thermal quarks and gluon propagators in two-color dense QCD, *Phys. Rev. D* **103**, 094008 (2021), [arXiv:2102.07231 \[hep-ph\]](#).
- [14] D. Suenaga and T. Kojo, Gluon propagator in two-color dense QCD: Massive Yang-Mills approach at one-loop, *Phys. Rev. D* **100**, 076017 (2019), [arXiv:1905.08751 \[hep-ph\]](#).
- [15] T. Kojo and G. Baym, Color screening in cold quark matter, *Phys. Rev. D* **89**, 125008 (2014), [arXiv:1404.1346 \[hep-ph\]](#).
- [16] R. Contant and M. Q. Huber, Dense two-color QCD from Dyson-Schwinger equations, *Phys. Rev. D* **101**, 014016 (2020), [arXiv:1909.12796 \[hep-ph\]](#).
- [17] R. Contant and M. Q. Huber, Phase structure and propagators at nonvanishing temperature for QCD and QCD-like theories, *Phys. Rev. D* **96**, 074002 (2017), [arXiv:1706.00943 \[hep-ph\]](#).
- [18] N. Strodthoff and L. von Smekal, Polyakov-Quark-Meson-Diquark Model for two-color QCD, *Phys. Lett. B* **731**, 350 (2014), [arXiv:1306.2897 \[hep-ph\]](#).
- [19] N. Strodthoff, B.-J. Schaefer, and L. von Smekal, Quark-meson-diquark model for two-color QCD, *Phys. Rev. D* **85**, 074007 (2012), [arXiv:1112.5401 \[hep-ph\]](#).
- [20] J. Schrieffer, *Theory Of Superconductivity*, Advanced Books Classics (Avalon Publishing, New York, 1999).
- [21] T. Boz, P. Giudice, S. Hands, and J.-I. Skullerud, Dense two-color QCD towards continuum and chiral limits, *Phys. Rev. D* **101**, 074506 (2020), [arXiv:1912.10975 \[hep-lat\]](#).
- [22] T. Boz, S. Cotter, L. Fister, D. Mehta, and J.-I. Skullerud, Phase transitions and gluodynamics in 2-colour matter at high density, *Eur. Phys. J. A* **49**, 87 (2013), [arXiv:1303.3223 \[hep-lat\]](#).
- [23] S. Cotter, P. Giudice, S. Hands, and J.-I. Skullerud, Towards the phase diagram of dense two-color matter, *Phys. Rev. D* **87**, 034507 (2013), [arXiv:1210.4496 \[hep-lat\]](#).
- [24] S. Hands, P. Kenny, S. Kim, and J.-I. Skullerud, Lattice Study of Dense Matter with Two Colors and Four Flavors, *Eur. Phys. J. A* **47**, 60 (2011), [arXiv:1101.4961 \[hep-lat\]](#).
- [25] S. Hands, S. Kim, and J.-I. Skullerud, A Quarkyonic Phase in Dense Two Color Matter?, *Phys. Rev. D* **81**, 091502 (2010), [arXiv:1001.1682 \[hep-lat\]](#).
- [26] S. Hands, P. Sitch, and J.-I. Skullerud, Hadron Spectrum in a Two-Colour Baryon-Rich Medium, *Phys. Lett. B* **662**, 405 (2008), [arXiv:0710.1966 \[hep-lat\]](#).
- [27] S. Hands, S. Kim, and J.-I. Skullerud, Deconfinement in dense 2-color QCD, *Eur. Phys. J. C* **48**, 193 (2006), [arXiv:hep-lat/0604004](#).
- [28] K. Iida, E. Itou, and T.-G. Lee, Two-colour QCD phases and the topology at low temperature and high density, *JHEP* **01**, 181, [arXiv:1910.07872 \[hep-lat\]](#).
- [29] K. Iida, E. Itou, and T.-G. Lee, Relative scale setting for two-color QCD with $N_f=2$ Wilson fermions, *PTEP* **2021**, 013B05 (2021), [arXiv:2008.06322 \[hep-lat\]](#).
- [30] S. Muroya, A. Nakamura, and C. Nonaka, Behavior of hadrons at finite density: Lattice study of color SU(2) QCD, *Phys. Lett. B* **551**, 305 (2003), [arXiv:hep-lat/0211010](#).
- [31] T. Makiyama, Y. Sakai, T. Saito, M. Ishii, J. Takahashi, K. Kashiwa, H. Kouno, A. Nakamura, and M. Yahiro, Phase structure of two-color QCD at real and imaginary chemical potentials; lattice simulations and model analyses, *Phys. Rev. D* **93**, 014505 (2016), [arXiv:1502.06191 \[hep-lat\]](#).

- [32] N. Astrakhantsev, V. Braguta, E. Ilgenfritz, A. Kotov, and A. Nikolaev, Lattice study of thermodynamic properties of dense QC_2D , *Phys. Rev. D* **102**, 074507 (2020), [arXiv:2007.07640 \[hep-lat\]](#).
- [33] N. Y. Astrakhantsev, V. G. Bornyakov, V. V. Braguta, E. M. Ilgenfritz, A. Y. Kotov, A. A. Nikolaev, and A. Rothkopf, Lattice study of static quark-antiquark interactions in dense quark matter, *JHEP* **05**, 171, [arXiv:1808.06466 \[hep-lat\]](#).
- [34] V. G. Bornyakov, V. V. Braguta, A. A. Nikolaev, and R. N. Rogalyov, Effects of Dense Quark Matter on Gluon Propagators in Lattice QC_2D , *Phys. Rev. D* **102**, 114511 (2020), [arXiv:2003.00232 \[hep-lat\]](#).
- [35] V. G. Bornyakov, V. V. Braguta, E. M. Ilgenfritz, A. Y. Kotov, A. V. Molochkov, and A. A. Nikolaev, Observation of deconfinement in a cold dense quark medium, *JHEP* **03**, 161, [arXiv:1711.01869 \[hep-lat\]](#).
- [36] V. V. Braguta, E. M. Ilgenfritz, A. Y. Kotov, A. V. Molochkov, and A. A. Nikolaev, Study of the phase diagram of dense two-color QCD within lattice simulation, *Phys. Rev. D* **94**, 114510 (2016), [arXiv:1605.04090 \[hep-lat\]](#).
- [37] V. V. Braguta, V. A. Goy, E. M. Ilgenfritz, A. Y. Kotov, A. V. Molochkov, M. Muller-Preussker, and B. Petersson, Two-Color QCD with Non-zero Chiral Chemical Potential, *JHEP* **06**, 094, [arXiv:1503.06670 \[hep-lat\]](#).
- [38] V. Braguta, M. N. Chernodub, V. A. Goy, K. Landsteiner, A. V. Molochkov, and M. I. Polikarpov, Temperature dependence of the axial magnetic effect in two-color quenched QCD, *Phys. Rev. D* **89**, 074510 (2014), [arXiv:1401.8095 \[hep-lat\]](#).
- [39] T. Boz, O. Hajizadeh, A. Maas, and J.-I. Skullerud, Finite-density gauge correlation functions in QC_2D , *Phys. Rev. D* **99**, 074514 (2019), [arXiv:1812.08517 \[hep-lat\]](#).
- [40] P. V. Buividovich, D. Smith, and L. von Smekal, Numerical Study of the Chiral Separation Effect in Two-Color QCD at Finite Density, (2020), [arXiv:2012.05184 \[hep-lat\]](#).
- [41] Z. Arzoumanian et al. (NANOGrav), The NANOGrav 11-year Data Set: High-precision timing of 45 Millisecond Pulsars, *Astrophys. J. Suppl.* **235**, 37 (2018), [arXiv:1801.01837 \[astro-ph.HE\]](#).
- [42] E. Fonseca et al., The NANOGrav Nine-year Data Set: Mass and Geometric Measurements of Binary Millisecond Pulsars, *Astrophys. J.* **832**, 167 (2016), [arXiv:1603.00545 \[astro-ph.HE\]](#).
- [43] P. Demorest, T. Pennucci, S. Ransom, M. Roberts, and J. Hessels, Shapiro Delay Measurement of A Two Solar Mass Neutron Star, *Nature* **467**, 1081 (2010), [arXiv:1010.5788 \[astro-ph.HE\]](#).
- [44] H. T. Cromartie et al., Relativistic Shapiro delay measurements of an extremely massive millisecond pulsar, *Nature Astron.* **4**, 72 (2019), [arXiv:1904.06759 \[astro-ph.HE\]](#).
- [45] E. Fonseca et al., Refined Mass and Geometric Measurements of the High-mass PSR J0740+6620, *Astrophys. J. Lett.* **915**, L12 (2021), [arXiv:2104.00880 \[astro-ph.HE\]](#).
- [46] J. Antoniadis et al., A Massive Pulsar in a Compact Relativistic Binary, *Science* **340**, 6131 (2013), [arXiv:1304.6875 \[astro-ph.HE\]](#).
- [47] B. Abbott et al. (LIGO Scientific, Virgo), GW170817: Observation of Gravitational Waves from a Binary Neutron Star Inspiral, *Phys. Rev. Lett.* **119**, 161101 (2017), [arXiv:1710.05832 \[gr-qc\]](#).
- [48] M. Miller et al., PSR J0030+0451 Mass and Radius from *NICER* Data and Implications for the Properties of Neutron Star Matter, *Astrophys. J. Lett.* **887**, L24 (2019), [arXiv:1912.05705 \[astro-ph.HE\]](#).
- [49] T. E. Riley et al., A *NICER* View of PSR J0030+0451: Millisecond Pulsar Parameter Estimation, *Astrophys. J. Lett.* **887**, L21 (2019), [arXiv:1912.05702 \[astro-ph.HE\]](#).
- [50] M. C. Miller et al., The Radius of PSR J0740+6620 from *NICER* and *XMM-Newton* Data, *Astrophys. J. Lett.* **918**, L28 (2021), [arXiv:2105.06979 \[astro-ph.HE\]](#).
- [51] T. E. Riley et al., A *NICER* View of the Massive Pulsar PSR J0740+6620 Informed by Radio Timing and *XMM-Newton* Spectroscopy, *Astrophys. J. Lett.* **918**, L27 (2021), [arXiv:2105.06980 \[astro-ph.HE\]](#).
- [52] G. Raaijmakers, S. K. Greif, K. Hebeler, T. Hinderer, S. Nissanke, A. Schwenk, T. E. Riley, A. L. Watts, J. M. Lattimer, and W. C. G. Ho, Constraints on the dense matter equation of state and neutron star properties from *NICER*'s mass-radius estimate of PSR J0740+6620 and multimessenger observations, (2021), [arXiv:2105.06981 \[astro-ph.HE\]](#).
- [53] T. Kojo, QCD equations of state and speed of sound in neutron stars, *AAPPS Bull.* **31**, 11 (2021), [arXiv:2011.10940 \[nucl-th\]](#).
- [54] K. Masuda, T. Hatsuda, and T. Takatsuka, Hadron-quark crossover and massive hybrid stars, *PTEP* **2013**, 073D01 (2013), [arXiv:1212.6803 \[nucl-th\]](#).
- [55] K. Masuda, T. Hatsuda, and T. Takatsuka, Hyperon Puzzle, Hadron-Quark Crossover and Massive Neutron Stars, *Eur. Phys. J. A* **52**, 65 (2016), [arXiv:1508.04861 \[nucl-th\]](#).
- [56] K. Masuda, T. Hatsuda, and T. Takatsuka, Hadron-quark crossover and hot neutron stars at birth, *PTEP* **2016**, 021D01 (2016), [arXiv:1506.00984 \[nucl-th\]](#).
- [57] K. Masuda, T. Hatsuda, and T. Takatsuka, Hadron-Quark Crossover and Massive Hybrid Stars with Strangeness, *Astrophys. J.* **764**, 12 (2013), [arXiv:1205.3621 \[nucl-th\]](#).
- [58] T. Kojo, P. D. Powell, Y. Song, and G. Baym, Phenomenological QCD equation of state for massive neutron stars, *Phys. Rev. D* **91**, 045003 (2015), [arXiv:1412.1108 \[hep-ph\]](#).
- [59] T. Kojo, Phenomenological neutron star equations of state: 3-window modeling of QCD matter, *Eur. Phys. J. A* **52**, 51 (2016), [arXiv:1508.04408 \[hep-ph\]](#).
- [60] K. Fukushima and T. Kojo, The Quarkyonic Star, *Astrophys. J.* **817**, 180 (2016), [arXiv:1509.00356 \[nucl-th\]](#).
- [61] G. Baym, T. Hatsuda, T. Kojo, P. D. Powell, Y. Song, and T. Takatsuka, From hadrons to quarks in neutron stars: a review, *Rept. Prog. Phys.* **81**, 056902 (2018), [arXiv:1707.04966 \[astro-ph.HE\]](#).
- [62] G. Baym, S. Furusawa, T. Hatsuda, T. Kojo, and H. Togashi, New Neutron Star Equation of State with Quark-Hadron Crossover, *Astrophys. J.* **885**, 42 (2019), [arXiv:1903.08963 \[astro-ph.HE\]](#).
- [63] T. Kojo, G. Baym, and T. Hatsuda, QHC21 equation of state of neutron star matter - in light of 2021 *NICER* data, (2021), [arXiv:2111.11919 \[astro-ph.HE\]](#).
- [64] A. Ayriyan, D. Blaschke, A. G. Grunfeld, D. Alvarez-Castillo, H. Grigorian, and V. Abgaryan, Bayesian analysis of multimessenger M-R data with interpolated hybrid EoS, *Eur. Phys. J. A* **57**, 318 (2021), [arXiv:2102.13485 \[astro-ph.HE\]](#).

- [65] T. Minamikawa, T. Kojo, and M. Harada, Quark-hadron crossover equations of state for neutron stars: constraining the chiral invariant mass in a parity doublet model, *Phys. Rev. C* **103**, 045205 (2021), [arXiv:2011.13684 \[nucl-th\]](#).
- [66] T. Minamikawa, T. Kojo, and M. Harada, Chiral condensates for neutron stars in hadron-quark crossover: from a parity doublet nucleon model to an NJL quark model, (2021), [arXiv:2107.14545 \[nucl-th\]](#).
- [67] L. McLerran and S. Reddy, Quarkyonic Matter and Neutron Stars, *Phys. Rev. Lett.* **122**, 122701 (2019), [arXiv:1811.12503 \[nucl-th\]](#).
- [68] L. McLerran and R. D. Pisarski, Phases of cold, dense quarks at large $N(c)$, *Nucl. Phys. A* **796**, 83 (2007), [arXiv:0706.2191 \[hep-ph\]](#).
- [69] L. McLerran, K. Redlich, and C. Sasaki, Quarkyonic Matter and Chiral Symmetry Breaking, *Nucl. Phys. A* **824**, 86 (2009), [arXiv:0812.3585 \[hep-ph\]](#).
- [70] A. Andronic et al., Hadron Production in Ultra-relativistic Nuclear Collisions: Quarkyonic Matter and a Triple Point in the Phase Diagram of QCD, *Nucl. Phys. A* **837**, 65 (2010), [arXiv:0911.4806 \[hep-ph\]](#).
- [71] L. Y. Glozman and R. F. Wagenbrunn, Chirally symmetric but confining dense and cold matter, *Phys. Rev. D* **77**, 054027 (2008), [arXiv:0709.3080 \[hep-ph\]](#).
- [72] A. M. Tselik and R. D. Pisarski, Low energy physics of interacting bosons with a moat spectrum, and the implications for condensed matter and cold nuclear matter, (2021), [arXiv:2103.15835 \[nucl-th\]](#).
- [73] Y. Hidaka, L. D. McLerran, and R. D. Pisarski, Baryons and the phase diagram for a large number of colors and flavors, *Nucl. Phys. A* **808**, 117 (2008), [arXiv:0803.0279 \[hep-ph\]](#).
- [74] T. Kojo, Y. Hidaka, L. McLerran, and R. D. Pisarski, Quarkyonic Chiral Spirals, *Nucl. Phys. A* **843**, 37 (2010), [arXiv:0912.3800 \[hep-ph\]](#).
- [75] T. Kojo, R. D. Pisarski, and A. M. Tselik, Covering the Fermi Surface with Patches of Quarkyonic Chiral Spirals, *Phys. Rev. D* **82**, 074015 (2010), [arXiv:1007.0248 \[hep-ph\]](#).
- [76] T. Kojo, A (1+1) dimensional example of Quarkyonic matter, *Nucl. Phys. A* **877**, 70 (2012), [arXiv:1106.2187 \[hep-ph\]](#).
- [77] T. Kojo, Y. Hidaka, K. Fukushima, L. D. McLerran, and R. D. Pisarski, Interweaving Chiral Spirals, *Nucl. Phys. A* **875**, 94 (2012), [arXiv:1107.2124 \[hep-ph\]](#).
- [78] E. J. Ferrer, V. de la Incera, and A. Sanchez, Quarkyonic Chiral Spirals in a Magnetic Field, *Acta Phys. Polon. Supp.* **5**, 679 (2012), [arXiv:1205.4492 \[nucl-th\]](#).
- [79] K. S. Jeong, L. McLerran, and S. Sen, Dynamically generated momentum space shell structure of quarkyonic matter via an excluded volume model, *Phys. Rev. C* **101**, 035201 (2020), [arXiv:1908.04799 \[nucl-th\]](#).
- [80] D. C. Duarte, S. Hernandez-Ortiz, and K. S. Jeong, Excluded-volume model for quarkyonic Matter: Three-flavor baryon-quark Mixture, *Phys. Rev. C* **102**, 025203 (2020), [arXiv:2003.02362 \[nucl-th\]](#).
- [81] D. C. Duarte, S. Hernandez-Ortiz, and K. S. Jeong, Excluded-volume model for quarkyonic matter. II. Three-flavor shell-like distribution of baryons in phase space, *Phys. Rev. C* **102**, 065202 (2020), [arXiv:2007.08098 \[nucl-th\]](#).
- [82] T. Zhao and J. M. Lattimer, Quarkyonic Matter Equation of State in Beta-Equilibrium, *Phys. Rev. D* **102**, 023021 (2020), [arXiv:2004.08293 \[astro-ph.HE\]](#).
- [83] G. Cao and J. Liao, A field theoretical model for quarkyonic matter, *JHEP* **10**, 168, [arXiv:2007.02028 \[nucl-th\]](#).
- [84] J. Margueron, H. Hansen, P. Proust, and G. Chanfray, Quarkyonic stars with isospin-flavor asymmetry, *Phys. Rev. C* **104**, 055803 (2021), [arXiv:2103.10209 \[nucl-th\]](#).
- [85] T. Kojo, Stiffening of matter in quark-hadron continuity, *Phys. Rev. D* **104**, 074005 (2021), [arXiv:2106.06687 \[nucl-th\]](#).
- [86] K. Fukushima, T. Kojo, and W. Weise, Hard-core deconfinement and soft-surface delocalization from nuclear to quark matter, *Phys. Rev. D* **102**, 096017 (2020), [arXiv:2008.08436 \[hep-ph\]](#).
- [87] T. T. Takahashi and Y. Kanada-En'yo, Hadron-hadron interaction from SU(2) lattice QCD, *Phys. Rev. D* **82**, 094506 (2010), [arXiv:0912.0691 \[hep-lat\]](#).
- [88] M. Hippert, E. S. Fraga, and J. Noronha, Insights on the peak in the speed of sound of ultradense matter, *Phys. Rev. D* **104**, 034011 (2021), [arXiv:2105.04535 \[nucl-th\]](#).
- [89] A. J. Leggett and S. Zhang, *The BCS-BEC Crossover and the Unitary Fermi Gas*, edited by W. Zwerger, Lecture Notes in Physics (Springer, Berlin Heidelberg, 2012) pp. 33–47.
- [90] M. M. Parish, *The BCS-BEC Crossover, Quantum Gas Experiments*.
- [91] A. De Rujula, H. Georgi, and S. Glashow, Hadron Masses in a Gauge Theory, *Phys. Rev. D* **12**, 147 (1975).
- [92] T. Hatsuda and T. Kunihiro, QCD phenomenology based on a chiral effective Lagrangian, *Phys. Rept.* **247**, 221 (1994), [arXiv:hep-ph/9401310](#).
- [93] B. Freedman and L. D. McLerran, Quark Star Phenomenology, *Phys. Rev. D* **17**, 1109 (1978).
- [94] B. A. Freedman and L. D. McLerran, Fermions and Gauge Vector Mesons at Finite Temperature and Density. 3. The Ground State Energy of a Relativistic Quark Gas, *Phys. Rev. D* **16**, 1169 (1977).
- [95] E. Annala, T. Gorda, A. Kurkela, J. Nättilä, and A. Vuorinen, Evidence for quark-matter cores in massive neutron stars, *Nature Phys.* **16**, 907 (2020), [arXiv:1903.09121 \[astro-ph.HE\]](#).
- [96] T. Gorda, A. Kurkela, R. Paatelainen, S. Säppi, and A. Vuorinen, Cold quark matter at N³LO: Soft contributions, *Phys. Rev. D* **104**, 074015 (2021), [arXiv:2103.07427 \[hep-ph\]](#).
- [97] T. Gorda, A. Kurkela, R. Paatelainen, S. Säppi, and A. Vuorinen, Soft Interactions in Cold Quark Matter, *Phys. Rev. Lett.* **127**, 162003 (2021), [arXiv:2103.05658 \[hep-ph\]](#).
- [98] E. S. Fraga, A. Kurkela, and A. Vuorinen, Neutron star structure from QCD, *Eur. Phys. J. A* **52**, 49 (2016), [arXiv:1508.05019 \[nucl-th\]](#).
- [99] A. Kurkela, E. S. Fraga, J. Schaffner-Bielich, and A. Vuorinen, Constraining neutron star matter with Quantum Chromodynamics, *Astrophys. J.* **789**, 127 (2014), [arXiv:1402.6618 \[astro-ph.HE\]](#).
- [100] A. Kurkela, P. Romatschke, and A. Vuorinen, Cold Quark Matter, *Phys. Rev. D* **81**, 105021 (2010), [arXiv:0912.1856 \[hep-ph\]](#).
- [101] Y. Fujimoto and K. Fukushima, Equation of state of cold and dense QCD matter in resummed perturbation theory, *Phys. Rev. D* **105**, 014025 (2022), [arXiv:2011.10891 \[hep-ph\]](#).
- [102] Y. Song, G. Baym, T. Hatsuda, and T. Kojo, Effective repulsion in dense quark matter from nonperturbative gluon exchange, *Phys. Rev. D* **100**, 034018 (2019),

[arXiv:1905.01005 \[astro-ph.HE\]](#).

[103] T. Kojo, Zero point energy of composite particles: The medium effects, *Phys. Rev. D* **101**, 036001 (2020), [arXiv:1811.07363 \[hep-ph\]](#).